İSTANBUL UNIVERSITY CERRAHPAŞA

ORIGINAL ARTICLE
Electrica 2024; 24(3): 826-836

Power Quality Enhancement using Integrated Control Technique Quantum Calculus-based Least Mean Fourth and Optimized Fractional Order Proportional-Integral-Derivative

Prashant Kumar[1], Sabha Raj Arya[2]

[1]School of Sustainability Studies, Symbiosis Skill and Professional University, Pune, India
[2]Department of Electrical Engineering, S. V. National Institute of Technology, Surat, Gujarat, India

Cite this article as: P. Kumar and S. Raj Arya, "Power quality enhancement using integrated control technique q-LMF and optimized FOPID," *Electrica*, 24(3), 826-836, 2024.

ABSTRACT

This article proposes the effectiveness of a Dynamic Voltage Restorer (DVR) based on Quantum Calculus-based Least Mean Fourth (q-LMF) for compensating the impact of grid voltage perturbation. The adaptive controlling technique q-LMF is utilized for the computation of the fundamental active load voltage component derived from the polluted grid voltage. The proposed technique is inspired by the conventional Least Mean Fourth (LMF) scheme with the addition of the "q" variable. The adaptation of "q" improves the performance of the controller. A modified complex coefficient filter is used to extract the filtered Point of Intersection (PoI) voltage under a disturbed grid. The DVR feeds the appropriate compensatory voltage at the PoI to minimize voltage disturbances and restores the load voltage magnitude. The capacitor voltage of the DC bus is stabilized with a Fractional Order PID, and its parameters are tuned with a Pelican optimizer. The proposed control technique has achieved significant advancement with quicker settling time (0.15 s), reduced overshoot (2.4%), and undershoot (5.6%). Furthermore, less compensated time of 0.008 s is required during a sag. The proposed DVR system is initially modeled in MATLAB/Simulink and corroborated using laboratory experimentation. Additionally, a comparative study is shown to justify the superiority of the proposed q-LMF over the Least Mean Square and LMF control methods in terms of weight oscillations, voltage THD, and statistical indices like rise time, settling time, and overshoot. The experimental results are carried out for the validation of the developed control strategy.

***Index Terms*—**Dynamic Voltage Restorer (DVR), filter, Fractional Order PID (FOPID), voltage disturbance, optimization

I. INTRODUCTION

The application of power electronic converters in connecting many Diesel Generators (DGs) with adjacent loads is a novel concept for a "microgrid" [1]. Power quality (PQ) issues in the distribution network are caused by the increased penetration of nonlinear loads such as diodes and thyristor-based circuits [2]. Power quality issues, reactive power burden, poor power factor (PF), voltage harmonics, current harmonics, and increased heating have decreased the system's overall efficiency [3]. Series Active Power Filter (SAPF) offers qualities such as customized filtering, more flexibility against system disturbances, and fast dynamical response and becomes an ideal solution for minimizing current-related PQ difficulties [4]. It is also noteworthy that active power filters operate more efficiently under light loads. Power quality concerns may be classified as current- or voltage-related difficulties, and they can cause malfunction of end-user equipment. The PQ issues associated with current are current harmonics, reactive power utilization, and inadequate power factor. The PQ aspects related to voltage include voltage sags, voltage swells, notches, voltage harmonics, flickers, and so on [5]. Q3

Several control strategies for SAPF have been discussed in the literature. The two most popular conventional control strategies are the Instantaneous Reactive Power Theory (IRPT) and theory of Synchronous Reference Frame (SRF) [6] [7]. These two control schemes are used to calculate the fundamental load component for reference current generation for SAPF. The IRPT control scheme is discussed for power conditioning. The SRF theory is also known as the dq theory because of its use of the phase-locked loop (PLL), and its foundation is based on the dq0 frame of reference. However, it is crucial to evaluate the SRF theory's efficacy in improving PQ aspects. The IRPT, on the contrary, incorporates computations in a fixed reference frame without the usage

Corresponding author:
Prashant Kumar

E-mail:
prashant2685@gmail.com

Received: September 24, 2024

Revision Requested: October 19, 2024

Last Revision Received: October 21, 2024

Accepted: October 29, 2024

Publication Date: November 8, 2024

DOI: 10.5152/electrica.2024.24127

of a PLL; as a result, it is widely used in the control of SAPF. The IRPT involves a much lower computation time as PLLs are not required. Some of the limitations of IRPT are sensitivity to harmonics, complexity of implementation, and dynamic response issues.

In ref. [8], the authors have illustrated PQ enhancement with fundamental estimation based on Artificial Neural Network (ANN) and DC voltage stabilization using an ANFIS controller. In papers [9] and [10], the fundamental direct load quantity extraction in shunt active filtering is achieved via a Hermite polynomial-based controller, and fuzzy-PI is implemented for voltage error regulation. In ref. [11], the authors proposed an enhanced filtering generalized integrator (EFGI)-based filtering technique to filter the source voltage from harmonic content. This control scheme improves the PQ issues in grid-tied PV systems. The control Least Mean Square (LMS) is commonly used as an adaptive controller in the Dynamic Voltage Restorer (DVR) operation [12]. It is an adaptive filter. The properties of the unknown system in which this filter is used, as well as environmental changes, have propelled adaptive filter theory to the forefront of research. It is also well known that the normal LMS algorithm produces significantly more noise in the weights than the LMF approach when the time constant values for both techniques are identical. Hence, the approach is to achieve the right learning rule that produces a lower steady-state error and excellent tracking as compared to the conventional LMS-based control system [13]. A typical smaller step size is recommended to achieve the lowest possible error rate. Equilibrium is essential to achieve a faster convergence rate (CR), a lower step size, and better control performance. It is investigated that if CR is less than zero or approaches zero, the CR is much better with better tracking capability as compared to CR equal to one [14]. Numerous academics have been drawn to changes in its control parameters. The most popular and widely employed LMS algorithms for enhancing PQ include variable step size LMS and Least Mean Mixed Norm [15]. These algorithms allow self-governing tracking, reduced real-time processing, robustness to changes in system parameters, and good response even under dynamic load conditions. The mixed-norm constraint-based improved proportionate normalized LMS fourth technique computes the fundamental quantity of weight from the disturbed grid voltage and computes the reference load voltage. In [16], a new family of q-LMF-based control-based stochastic gradient algorithms for channel identification is proposed. The q-Least Mean Fourth (q-LMF) method, using q-calculus, also referred to as Jackson's derivative, expands the LMF technique even further. The q-LMF algorithm has also been applied to the development of whitening filters and system identification. The suggested algorithm in this study provides a new way to correlate error correlation energy to give a quick CR, enhanced stability, and reduced steady-state error [17]. The proposed technique modifies the LMF approach to reduce the fourth power of the instantaneous error estimate. The weighted sum of the inputs is sent to the summation unit. If the estimated output differs from the desired output, the weights are adjusted based on the obtained errors. Based on the error, the q-LMF learning algorithm adjusts the weight. To minimize errors and update weights, a q-LMF adaptive learning filter is utilized. The step size influences how fast the q-LMF converges. The proposed q-LMF is used for extracting the fundamental load component of each phase of the system, and further used to generate reference load voltage for each phase. Different controlling schemes were studied for the stabilization of DC-link voltage. Most researchers have implemented conventional techniques to minimize the capacitor voltage oscillations like PI and Proportional-Integral-Derivative (PID). The PID Controller is ineffective in handling the parameter variations [18] and this leads to deviation from the set value. Proportional-Integra l-Derivative has a limitation of three gain variables which need to be adjusted to achieve the desired response. This also restricts the system's applications under a dynamic state. The Fractional Order PID (FOPID) is suggested to surmount this limitation since the controller has a feature of five-degree freedom. The extra knob tuning variables are available to achieve fine-tuned gain values and the tuning mechanism is integrated with a metaheuristic approach. This strengthens the tuning and researchers have given equal importance to choosing the optimizer. Myriads of optimization techniques are studied in the literature such as Harris's Hawks Optimizer [19], the Path Finder Algorithm [20], and controller PI-FOPID optimized with the Gorilla Troops Optimizer [21] and have been extensively employed by intellectuals to obtain improved system stability. In this study, the authors have incorporated Pelican optimization. This pelican is motivated based on hunting and has higher exploitation to achieve the global optimum solution. Pelican optimizer is superior and more competitive as it converges quickly and avoids local minima trapping.

The significant highlights of the research study are as follows:

1. This paper proposes the extraction of fundamental quantity from disturbed grid voltage with q-LMF and Pelican-based FOPID, provided for capacitor voltage stabilization.
2. The proposed DVR is assessed under different voltage grid issues, and its performance is evaluated using time response characteristics like rise time, settling time, and peak overshoot.
3. A comparison of the suggested Pelican-FOPID performance is conducted over LMS-PI and LMF-PI to demonstrate its superiority.
4. The efficacy of the q-LMF and optimized FOPID is also demonstrated by comparing its weight converging performance with other optimizers like LMS and LMF.
5. The DVR experimental hardware results are evaluated under grid voltage sag, swell, imbalance, and distortion scenarios. The system load voltage is restored with reduced voltage total harmonic distortion (THD) below 5% as per the IEEE 519 standard.

II. SYSTEM CONFIGURATION

The proposed layout includes mostly a 3∅ VSC, a DC link capacitor (C_{dc}), interface inductor (L_f), source impedance (Rs, Ls), and ripple filter as shown in Fig. 1.

There are six insulated gate bipolar transistors (IGBTs) in the converter (VSC). The VSC is linked to the PoI employing an interface inductor (L_f). The gate signals for VSC switches are extracted through a proper control scheme designed based on the q-LMF algorithm. The total active load voltage is estimated by subtracting the fundamental weight with the DC-link loss component. The resulting output is then multiplied by the unit template of each phase to obtain the reference load voltage. The six switching signals are generated after comparing the three-reference load voltage with the actual load voltage.

III. CONTROL ALGORITHM

The proposed article utilizes a q-LMF-based control scheme to find the fundamental quantity of nonlinear load current. The control scheme is developed using a mathematical model with a suitable

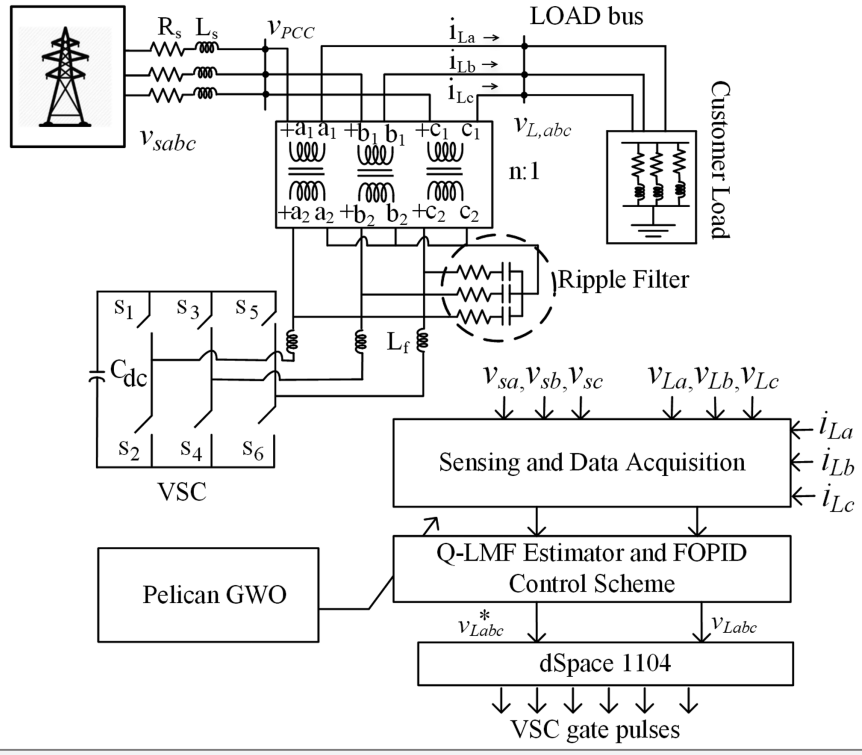

Fig. 1. Proposed circuit diagram. It includes the component connections and sensed signal for estimating the reference load voltage signal.

step size. By employing an extra control parameter q, the proposed q calculus-based LMF can be used to improve the performance of the traditional LMF while maintaining the algorithm's stability. Furthermore, the proposed control technique generates adaptive weight values. If $q = 1$, the proposed q-LMF algorithm acts as a conventional LMF [16] [17]. However, the change in the q parameter can alter the behavior of the algorithm entirely. The adaptation and fundamental estimation strategy is depicted in Fig. 2.

A. Introduction to q-Calculus

Quantum calculus is often known as limitless calculus. The derivative of a function is expressed as follows:

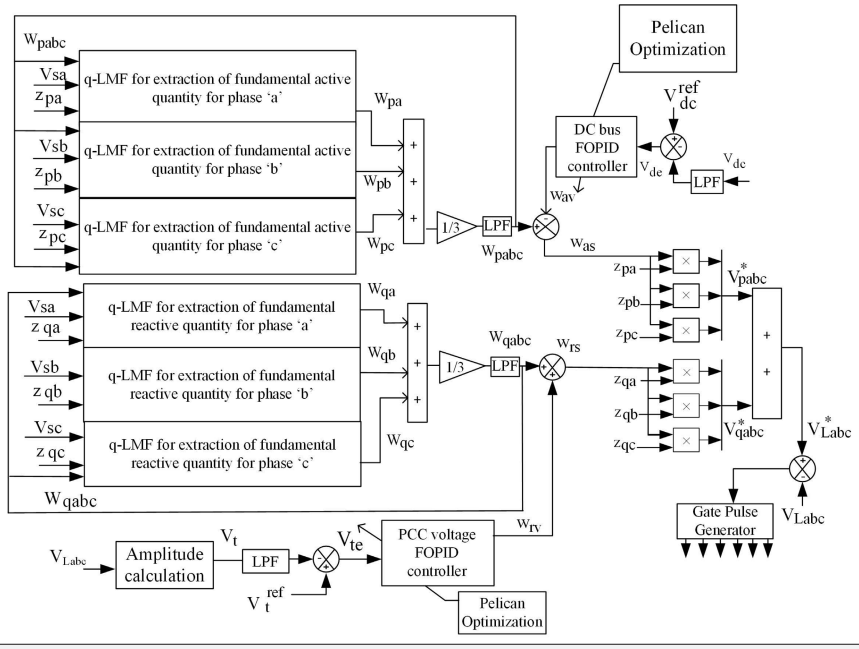

Fig. 2. Estimation of load reference voltage includes the complete operation of the control algorithm for the estimation of reference load voltage from the polluted grid voltage.

$$d_q(f(x)) = f(qx) - f(x) \tag{1}$$

The derivative of (1) is given as follows:

$$D_q(f(x)) = \frac{d_q(f(x))}{d_q(x)} = \frac{f(qx) - f(x)}{(q-1)x} \tag{2}$$

If q tends to 1, the above expression is suited to the classical derivative. The q-gradient of function $f(x)$ for "m" number of variables is expressed as follows [16]:

$$\begin{aligned} &\nabla_{q,w} f(x) \quad [D_{q1,x1} f(x), D_{q2,x2} f(x), ..., D_{qn,xm} f(x)]^T \\ &q = [q_1, q_2, ..., q_m]^T \end{aligned} \tag{3}$$

B. Proposed Adaptive q-LMF Algorithm

The conventional LMF algorithm is expressed in (4):

$$W(n+1) = W(n) - \frac{\lambda}{4} \nabla_w J_k \tag{4}$$

where "λ" is the step size or learning rate, J_k is the cost function for the proposed q-LMF algorithm, and it is expressed as $J_k = e^4(n)$. Here, $e(n)$ is defined as the calculated error between the actual output (d) and the calculated output ($W^T(n)$ x (n)) at the nth instant. Also, $x(n)$ is denoted as the input signal, which is expressed as: $x(n) = [x_1, x_2, ..., x_C]^T$.

$$e(n) = d(n) - W^T(n) x(n) \tag{5}$$

and "W" is the weights vector, and "C" is the length of the filter. The suggested q-LMF algorithm is obtained with the q-gradient [21].

$$W(n+1) = W(n) - \frac{\lambda}{4} \nabla_{q,w} J_k \tag{6}$$

$$\nabla_{q,w} J_k = -4E(q_i^3 + q_i^2 + q_i^2 + 1) x_i(n) e^3 \quad i = 1, 2, 3, ..., C \tag{7}$$

$$\nabla_{q,w} J_k = -4E(Mx(n) e^3(n)] \tag{8}$$

Where q_i is the quiescent value at kth instant of time, M is a diagonal matrix.

$$diag(M) = \left[\left(\frac{q_1^3 + q_1^2 + q_1^3}{4} \right), \left(\frac{q_2^3 + q_2^2 + q_2 + 1}{4} \right), ..., \left(\frac{q_c^3 + q_c^2 + q_c + 1}{4} \right) \right]^T \tag{9}$$

Because of system ergodicity, $\nabla_{q,w} J_k$ can be expressed as:

$$\nabla_{q,w} J_k \approx -4Mx(n) e^3(n) \tag{10}$$

Equation (6) will be expressed as:

$$w(n+1) = w(n) + \lambda M x(n) e^3(n) \tag{11}$$

The input variable $x(n)$ is given by:

$$x(n) = [z_{pa} \; z_{pb} \; z_{pc}]^T \tag{12}$$

$$e(n) = \begin{bmatrix} v_{sa}(n) - z_{pa} W_{pa}(n) \\ v_{sb}(n) - z_{pb} W_{pb}(n) \\ v_{sc}(n) - z_{pc} W_{pc}(n) \end{bmatrix} \tag{13}$$

$$W(n+1) = [W_{pa}(n+1) \; W_{pb}(n+1) \; W_{pc}(n+1)]^T \tag{14}$$

$$W(n) = [W_{pa}(n) \; W_{pb}(n) \; W_{pc}(n)]^T W \tag{15}$$

Where in-phase unit templates are represented by z_{pa}, z_{pb}, and z_{pc}. $e(n)$ denotes the error between the actual and measured weight component.

The weight of the fundamental direct quantity of the voltage of phase "a," "b," and "c" is expressed as:

$$\left.\begin{aligned} W_{pa}(n+1) &= W_{pa}(n) + \lambda M((z_{pa}(n))^3) \\ W_{pb}(n+1) &= W_{pb}(n) + \lambda M((z_{pb}(n))^3) \\ W_{pc}(n+1) &= W_{pc}(n) + \lambda M((z_{pc}(n))^3) \end{aligned}\right\} \tag{16a}$$

For LMF-based operations, $M = [1\ 1\ 1]^T$

While for q-LMF, the value of q can be chosen according to the requirement $q = 2, 3, 4$……

For $q_1, q_2, q_3 = 2$,

$M = [3.5\ 3.5\ 3.5]$ using (9)

Hence, the M matrix is dependent on the choice of q.

The arithmetic mean weight (W_{pabc}) of all the active components is obtained by adding (16a).

$$W_{pabc} = avg(W_{pa}, W_{pb}, W_{pc}) \tag{16b}$$

Similarly, the errors and fundamental weights of phases a, b, and c are computed for the arithmetic mean of the reactive weight (W_{qabc}) given as,

$$W_{qabc} = avg(W_{qa}, W_{qb}, W_{qc}) \tag{16c}$$

The mCCF is used to obtain a sinusoidal unit template under abnormal grid conditions. The transfer function of mCCF is given by (17).

$$Y(s) = w_c \frac{s + w_c + jw_o}{(s + w_c)^2 + w_o^2} \tag{17}$$

where ω_c and ω_o is the bandwidth of CCF and the favorable angular frequency of CCF, respectively. The values selected for where ω_c, ω_o are 94.2 and 314 rad/s.

IV. VOLTAGE ERROR REGULATION USING PELICAN-OPTIMIZED FRACTIONAL ORDER PID

Better voltage regulation performance of DC and AC links is provided by the proposed FOPID controller ($PI^{\alpha}D^{\beta}$), which is based on the optimization technique for DVR systems. The proposed Pelican Optimization optimizes the variables of the FOPID controller to provide more stabilized voltage across the DC and AC links. The concept of the proposed Pelican optimizer is based on the pelican's behavior and planned strategy during the attacking mechanism and hunting prey to provide updated candidate solutions [22]. This strategy of hunting is performed in two simulated stages.

(i) Exploration state means moving toward prey.
(ii) Exploitation state means winging on the surface of water.

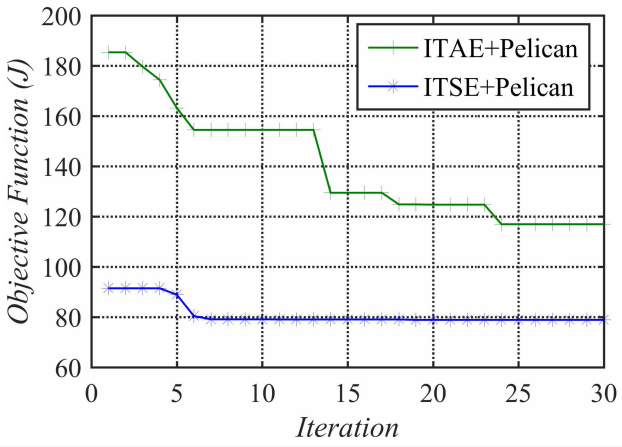

Fig. 3. Convergence characteristics of the integral time square error and integral of time-weighted absolute error with the Pelican Optimizer. The selection of the fitness function to analyze the performance of the Fractional Order PID.

The recommended FOPID is evaluated based on the ITSE objective function.

The integral time square error (ITSE) will be utilized to find the tuned gain values of FOPID. The performance time index can be represented in (18).

$$Cost\ function\,(J_1) = ITSE = \int_0^{T_S} t \cdot \left(e^2(k)\right) \cdot dt \tag{18}$$

where $e(k)$ is the error signal and $t(k)$ is the time vector.

The objective function (J_1) refers to ITSE. The simulation results have been presented with a convergence characteristic of 30 runs and observed that more error is associated with ITAE compared to ITSE, as shown in Fig. 3. Integral time square error + Pelican provides faster convergence and a lower objective function of error value than integral of time-weighted absolute error (ITAE) ITAE + Pelican algorithms. Hence, the ITSE function is considered to obtain the optimum gain values of the FOPID controller.

The performance of the Pelican algorithm is depicted in Fig. 4a and 4b. This converging behavior is against the iterations for confirming the optimal gain values during DVR operation.

The costing function of DC FOPID is achieved at the 23rd iteration with a value of 33.119618, and ACFOPID is settled at the 42nd iteration with 102.0308. Direct current and AC link gain values, through trial-and-error approach and the proposed Pelican-FOPID method, are enlisted in Table I.

A. Estimation of Unit Voltage Vector and Quadrature Unit Template

The complete description and application are discussed in ref. [18]. The transient responsiveness is examined using a Pelican-based FOPID controller in DVR systems. The computed error (V_{de}) is given as input to FOPID controller, enhancing the voltage regulation and achieving the reference set values [18].

The DC link error value is $V_{de} = V_{dc}^{ref} - V_{dc}$ (19a)

The response of FOPID (W_{av}) and active fundamental quantity (W_{pabc}) is utilized to obtain (w_{as}), as given in (19b).

$$w_{as} = W_{pabc} - w_{av} \tag{19b}$$

The load quantity computation for the terminal voltage (V_t) is depicted in (20a). The generated voltage error value between the actual and reference values is fed as an input to the FOPID controller and maintains the AC link voltage level.

$$V_{te} = V_t^{ref} - V_t \tag{20a}$$

Where $V_t = \sqrt{0.667(V_{LA}^2 + V_{LB}^2 + V_{LC}^2)}$ (20b)

The response of FOPID (w_{rv}) and reactive fundamental quantity (W_{qabc}) to achieve (w_{rs}), as expressed in (21).

$$w_{rs} = W_{qabc} + w_{rv} \tag{21}$$

A unit and quadrature vector can be calculated as follows [4-6]:

$$z_{pa} = \frac{i_{la}}{i_{pt}}; z_{pb} = \frac{i_{lb}}{i_{pt}}; z_{pc} = \frac{i_{lc}}{i_{pt}} \tag{22a}$$

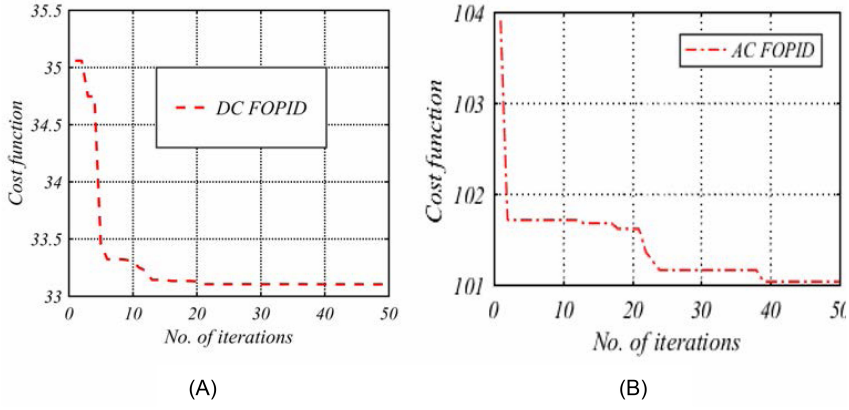

Fig. 4. Convergence analysis using Pelican algorithm (a) direct current link voltage (b) alternate current link voltage. This depicts the convergence value at which iteration the optimal gain values should be selected.

TABLE I. FOPID GAIN TUNNED RESPONSES

	Parameters									
	DC FOPID-Pelican Controller					AC FOPID-Pelican Controller				
Methods	K_{p1}	K_{i1}	K_{d1}	λ_1	δ_1	K_{p2}	K_{i2}	K_{d2}	λ_2	δ_2
Trial & error	32	0.52	0.001	1	1	0.92	1.24	0.03	1	1
Pelican-FOPID	45.2345	0.9883	0.4542	0.1032	0.9311	15.306	1.98	1.99	0.5911	0.1215

$$z_{aq}=\frac{z_{pc}-z_{pb}}{\sqrt{3}};z_{bq}=\frac{3z_{pc}+z_{pb}-z_{pc}}{2\sqrt{3}};z_{cq}=\frac{-3z_{pa}+z_{pb}-z_{pc}}{2\sqrt{3}} \quad (22b)$$

Where, $i_{pt}=\sqrt{\frac{2}{3}(i_{la}^2+i_{lb}^2+i_{lc}^2)}$.

Reference direct and quadrature components are evaluated with template weight vectors using (23).

$$\left.\begin{aligned} v_{pa}^{*}=w_{as}\times z_{pa};v_{pb}^{*}=w_{as}\times z_{pb};v_{pc}^{*}=w_{as}\times z_{pc}\\ v_{qa}^{*}=w_{rs}\times z_{qa};v_{qb}^{*}=w_{rs}\times z_{qb};v_{qc}^{*}=w_{rs}\times z_{qc}\end{aligned}\right\} \quad (23)$$

The extracted reference voltage by q-LMF and FOIPD controller and errors are computed by comparing with the actual supply voltage and reference value to develop the gating pulses for the series converter (V_{sc}) and expressed as follows:

$$e_a^{'}=v_{La}^{*}-v_{La};e_b^{'}=v_{Lb}^{*}-v_{Lb};e_c^{'}=v_{Lc}^{*}-v_{Lc} \quad (23)$$

The optimized controller values used for simulation and experimental are depicted in Appendix A.

V. RESULTS ANALYSIS

Fig. 5 illustrates the suggested system's operation under voltage sag, swell, distorted grid, imbalance, and compensation mechanism. The proposed control mechanism keeps the DC link voltage at its reference level. As shown in Fig. 5, a voltage sag of −20% magnitude is created at a timeframe of 0.4–s 0.46 s; at 0.5–0.56 s, a voltage swelling of +20%. A voltage distortion in supply voltage is introduced within a time frame of 0.6–0.66 s. Similarly, voltage unbalances of −20% are injected into the system with a timeframe of 0.7–0.76 s, as shown in Fig. 5. The fundamental weight estimation based on q-LMF employed to compute the reference load voltage for DVR is discussed here. The voltage signal shown in Fig. 5 is used to generate the reference load voltage for the DVR. These signals include supply voltages (v_{sabc}), injected voltage component (v_{inj}), and load current (i_{Labc}) of three individual phases. The voltage injected by series VSC is taken from the same DC bus voltage to retain the load end voltage at the desired sinusoidal value without any additional voltage support. To restore the load voltage after compensating for a voltage sag at the supply side, Fig. 6 illustrates the DVR's compensation response time of 0.008 s and represents an effective restoration of the load voltage.

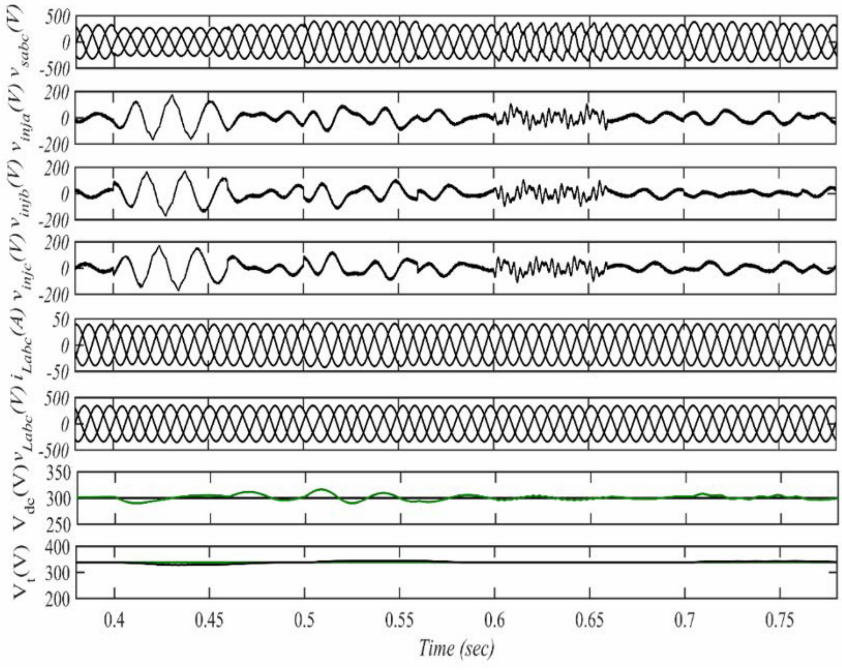

Fig. 5. Dynamical performances of Dynamic Voltage Restorer using the proposed control scheme. This includes the compensation characteristics of voltage issues in supply voltage and restores the set load voltage.

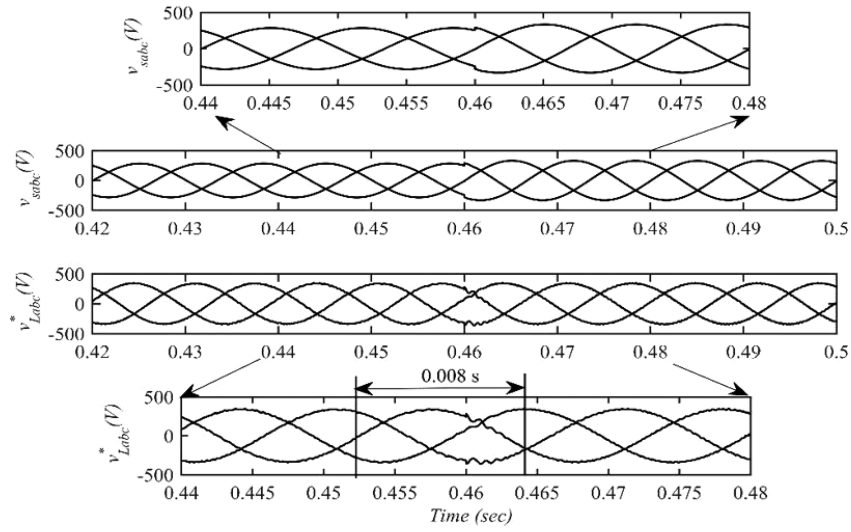

Fig. 6. Compensatory time response behavior during voltage sag in supply, with time taken to compensate for the voltage issues and return to a normal state.

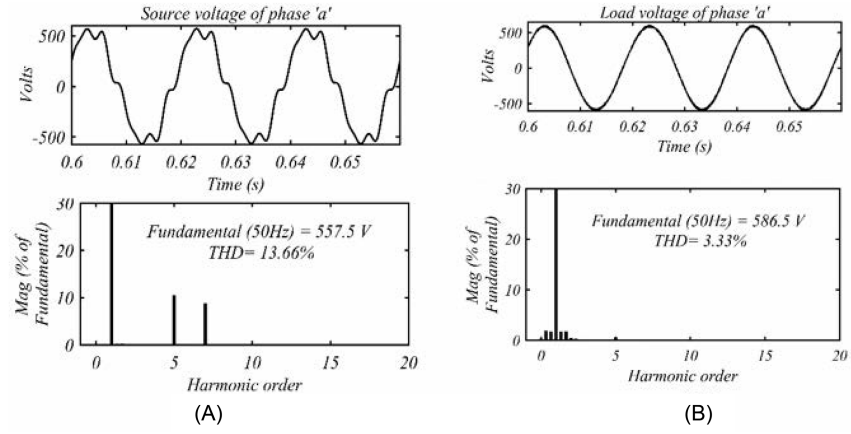

Fig. 7. Harmonic spectrum analysis. Voltage distortion analysis before and after inserting harmonics.

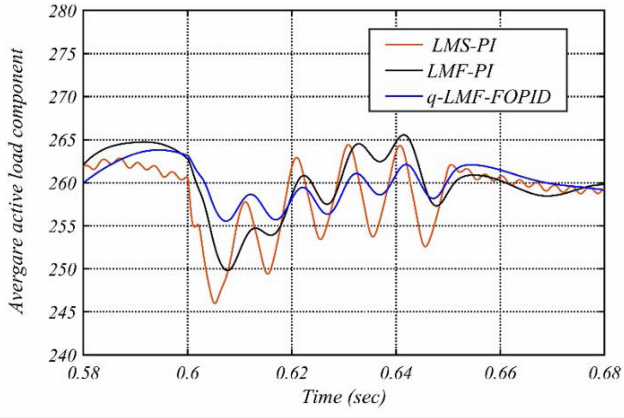

Fig. 8. Comparative convergence of standard least mean square-PI, least mean fourth-PI with proposed q-least mean fourth-FOPID. Validation of performance during weight convergence of different algorithms.

The THD of the distorted supply voltage (v_{sa}) is 13.66%, while the load voltage (v_{La}) after THD compensation is 3.33% at 585.4 V, with a peak value of 415V_{rms} which is below the IEEE-519 standards' allowable limit. The steady-state performance is corroborated by the harmonic spectrum analysis using q-LMF and Pelican FOPID control, and the results for harmonic distortion are given in Fig. 7. These figures show the harmonic spectrum of phase "a".

A. COMPARISON OF THE PROPOSED Q-LEAST MEAN FOURTH-BASED CONTROL WITH CONVENTIONAL ADAPTIVE CONTROL ALGORITHMS

Fig. 8 shows the average active weight of the fundamental component waveform under dynamic conditions. It is found that the fundamental weight signal converges fast with the q-LMF-FOPID-based algorithm, shown by blue color and has smaller oscillations as compared to the LMS-PI and LMF-PI methods, indicated by green and red color therefore tracking with convergence capability is found to be improved and faster under dynamics. The comparative performances of the two algorithms are summarized in Table II. It is evident from Fig. 8 that increasing q can lead to faster learning and less MSE.

TABLE II. COMPARISON OF STANDARD FLMS WITH PROPOSED MA-FLMS

S.N	Criteria	Standard LMS-PI	LMF-PI	Proposed q-LMF
1	Accuracy	Moderate	Moderate	Better
2	Converging speed	Slower	Good	Better
3	Complexity type	Moderate	Moderate	Moderate
4	Filter type	Adaptive	Adaptive	Adaptive
5	Static error	High	Relatively Low	Least
6	Dynamical state oscillations	High	Relatively Low	Low

However, in a nutshell, the comparative performances of the three algorithms in terms of weight oscillations and fitness function are discussed. Thus, the adaptive techniques such as standard LMS-PI and LMF-PI have large oscillations compared to q-LMF-FOPID. Due to small oscillations and lower MSE value, the proposed q-LMF algorithm is more stable than standard LMS-PI and LMF-PI especially under PQ distortion conditions. The time response nature of the DC link voltage is portrayed in Fig. 9 for the performance evaluation of the FOPID control algorithm. The FOPID coefficients are optimized by the Pelican, which maintains the DC link voltage at the reference level of 300V. It is observed that the DC link voltage has been settling to a 2% tolerance range of 294–306 V within 0.223 s and improves the overall DVR performance. Table III indicates the dynamic response indicators such as settle time, peak overshoot, and undershoot.

VI. EXPERIMENTAL RESULT

A hardware setup is developed in the laboratory using Hall Effect current and voltage sensors LEM LA 25P and LEM LV 25P, respectively, as shown in Fig. 10. Sensor circuits measure each phase's source voltage, load voltage, DC link voltage, and source voltage. A PQ analyzer (Fluke-43B) is utilized for harmonic spectra analysis of

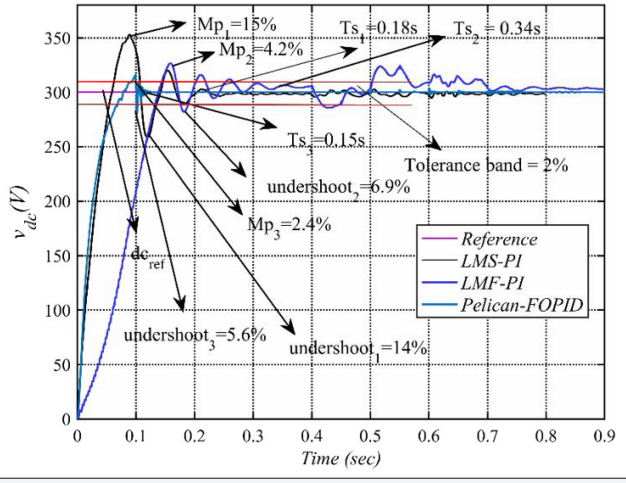

Fig. 9. Comparative direct current-link voltage response. Transitory time response characteristics and soughting the performance in terms of settle time, overshoot, and undershoot.

TABLE III. TRANSIENT TIME RESPONSE OF DIRECT CURRENT LINK

Control Scheme Parameters	LMS-PI [14]	LMF-PI [15]	Optimize FOPID
Settle time (t_s), (s)	0.18	0.34	0.15
Maximum overshoot (M_p), (%)	15	4.2	2.4
Undershoot (U_s), (%)	14	6.9	5.6

current and voltage. For voltage and current measurements, voltage probes and current probes (Agilent made) are used. The dynamic response of the proposed system is captured using a digital signal oscilloscope (DSOX2014A). Also, the effectiveness of the proposed system is evaluated by experimenting with the proposed system in a hardware prototype.

A. Experimental Performance of Three-Phase Three-Wire DVR

The experimental performance of DVR is presented under the voltage distortion event. The efficacy of the control algorithm efficacy is demonstrated by using the distortion event. THD distortions of about 10% are introduced in the supply side voltage (v_{sabc}), as demonstrated in Fig. 11a, the corresponding compensated load voltage (v_{Labc}) is restored to its desired level of 110 V RMS without any distortions. The details of distortions compensation are determined by the supply voltage (v_{sa}), injection voltage (vinj), load side voltage (v_{La}), and load side current (*iLa*) of phase "a". During compensation of distortion, a DC link (V_{dc}) is maintained to achieve the set load voltage level as illustrated in Fig. 11b. Fig. 11(c) illustrates the effectiveness of DC link voltage (V_{dc}), terminal voltage (V_t), and load current (i_{La}) along with sag in supply voltage (v_{sab}) under various PQ.

The voltage distortion on the supply side is shown in Fig. 12(a–l). Fig. 12(a–c) shows the uncompensated source voltage (v_{sabc}) wave shapes and values for individual phases are 102.8 V, 101.4 V, and 102.9 V, and source current (i_{sa}). Total Harmonic Distortion voltage values for the supply line are 10.1%, 10.6%, and 10% as shown in Fig. 12(d–f). The load side voltages (v_{Labc}) measured after mitigation are 110.4 V, 110.2 V, and 110 V as shown in Fig. 12(g–i) with the load current (i_{La}). The compensated THD values are 4.4%, 4.7%, and 4% as presented in Fig. 12(j–l).

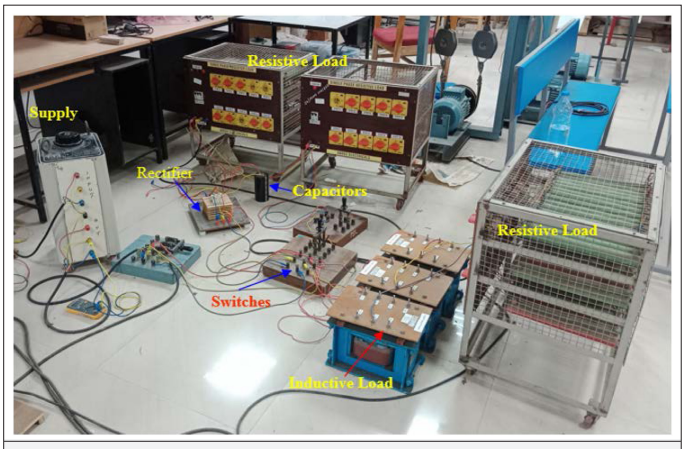

Fig. 10. Experimental setup to demonstrate result validation, including the result validation, includes the real-time prototype for incorporating the developed control algorithm.

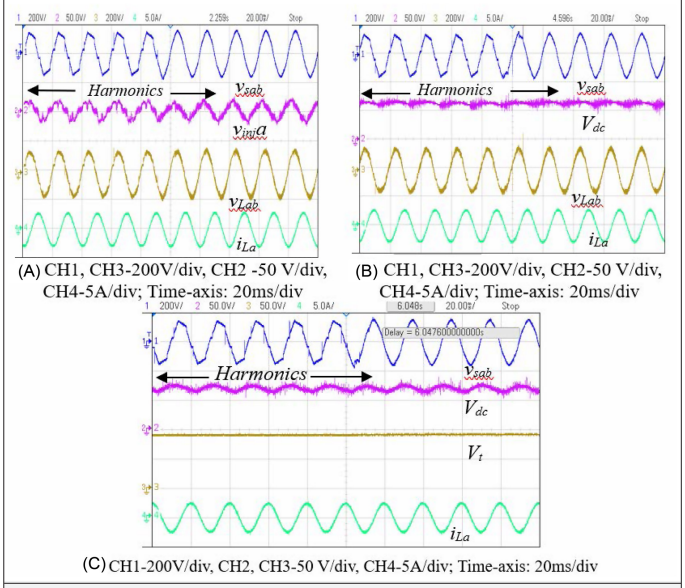

Fig. 11. Dynamic compensation performance of DVR during distortion (a) v_{sab},v_{inj},v_{Lab},i_{La}, (b) v_{sab},V_{dc},v_{Lab},i_{La}, and (c) v_{sab},V_{dc},V_t,i_{La}. Validating dynamical performance of the developed control algorithm under grid voltage distortion conditions.

VII. CONCLUSION

The proposed control scheme is based on the q-LMF and FOPID adaptive technique. The proposed control scheme is developed and implemented on a developed DVR prototype system. A new hybrid learning process in all the predictive models is used to obtain the optimal solution to the available voltage problem. The proposed control scheme includes an extra parameter q and offers more control over the dynamic performance and rate of convergence. The conventional LMS and LMF is also compared with the q-LMF for PQ improvement. The simulation and experimental results have shown that the THD of the load voltage is well within 5% as per IEEE—519: 2014 limits. The response of the proposed controller has proven to be effective and reliable compared with existing conventional techniques. The effectiveness of the proposed q-LMF-based control technique has smaller weight oscillations with a fast CR and the least steady-state error in the estimation of the fundamental active weight component. The MSE obtained with q-LMF showed a lower value than the conventional LMS and LMF control. Significant improvement for DC link voltage stabilization is sought in terms of time response such as less peak overshoot (2.4%), undershoot (5.6%), and quick settling time (0.15s) using the proposed control technique. Also, the oscillations are low in the proposed control technique compared to the LMS-PI and LMF-PI methods. The following gaps are the future research areas in the field of DVR.

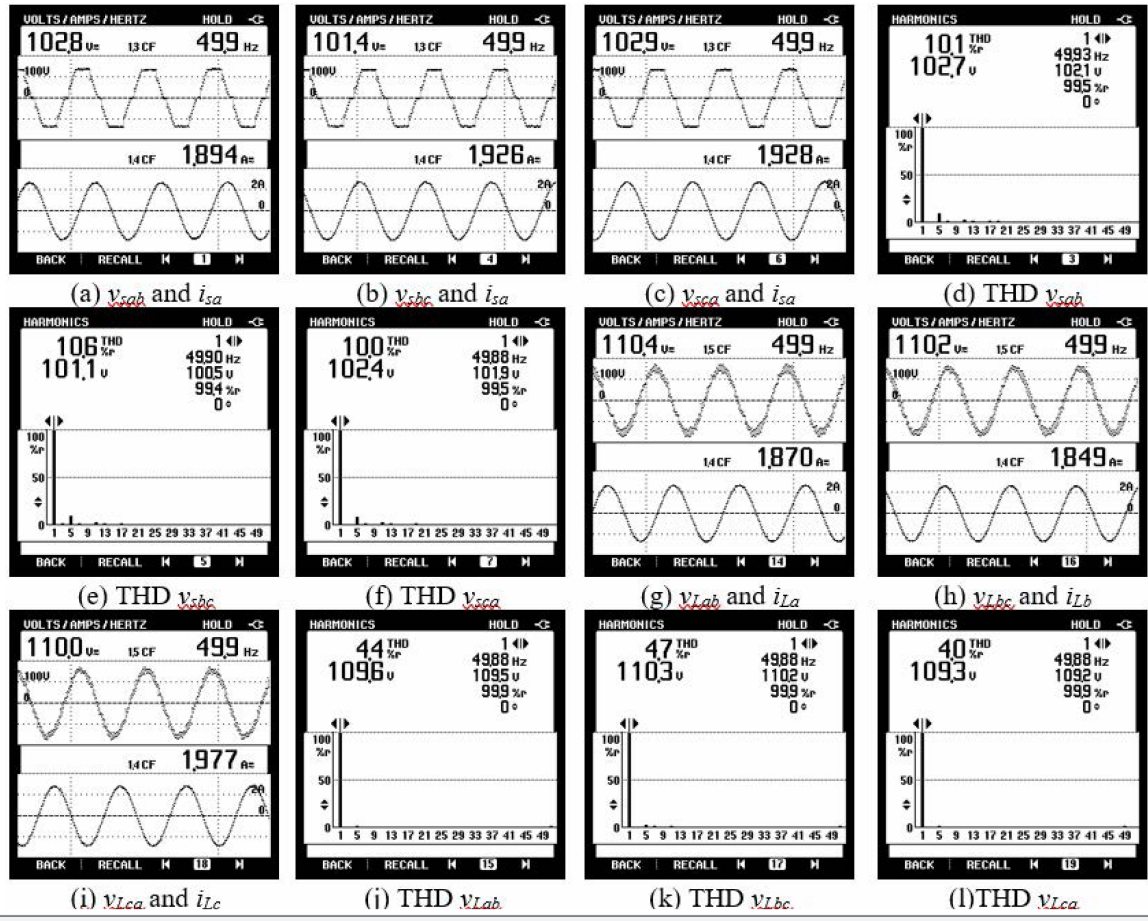

Fig. 12. Performance analysis of DVR under steady-state using q-LMF control algorithm with voltage distortion. Validation of steady-state performance with developed control algorithm.

1. To determine the feasibility of DVR integration with renewable energy and address the gird voltage PQ issues.
2. There should be more research done on the best way to build DVRs, particularly on the converter topology and the variety of advanced optimization methods for gain tuning.

Availability of Data and Materials: The data that support the findings of this study are available on request from the corresponding author.

Peer-review: Externally peer-reviewed.

Author Contributions: Concept – P.K.; Design – P.K.; Supervision – S.R.A.; Resources – P.K.; Materials – P.K.; Data Collection and/or Processing – P.K.; Analysis and/or Interpretation – P.K.; Literature Search – P.K.; Writing – P.K.; Critical Review – P.K.

Declaration of Interests: The authors have no conflict of interest to declare.

Funding: The authors declared that this study has received no financial support.

REFERENCES

1. H. Hafezi, and R. Faranda, "Dynamic voltage conditioner: A new concept for smart low-voltage distribution systems," *IEEE Trans. Power Electron.*, vol. 33, no. 9, pp. 7582–7590, 2017. [CrossRef]
2. A. K. Jindal, A. Ghosh, and A. Joshi, "Critical load bus voltage control using DVR under system frequency variation," *Electr. Power Syst. Res.*, vol. 78, no. 2, pp. 255–263, 2008. [CrossRef]
3. M. F. Kangarlu, E. Babaei, and F. Blaabjerg, "A comprehensive review of dynamic voltage restorers," *Int. J. Electr. Power Energy Syst.*, vol. 92, pp. 136–155, 2017. [CrossRef]
4. K. Chandrasekaran, and V. K. Ramachandaramurthy, "An improved dynamic voltage restorer for power quality improvement," *Int. J. Electr. Power Energy Syst.*, vol. 82, pp. 354–362, 2016. [CrossRef]
5. Y. Pal, A. Swarup, and B. Singh, "A review of compensating type custom power devices for power quality improvement," in *Proc. Joint International Conference on Power System Technology and IEEE Power India Conference*, 2008, pp.1–8. [CrossRef]
6. P. Kanjiya, B. Singh, A. Chandra, and K. Al-Haddad, "SRF theory revisited to control self-supported dynamic voltage restorer (DVR) for unbalanced and nonlinear loads," *IEEE Trans. Ind. Appl.*, vol. 49, no. 5, pp. 2330–2340, 2013. [CrossRef]
7. M. Pradhan, and M. K. Mishra, "Dual P-Q Theory based energy-optimized dynamic voltage restorer for power quality improvement in a distribution system," *IEEE Trans. Ind. Electron.*, vol. 66, no. 4, pp. 2946–2955, 2019. [CrossRef]
8. S. Vinnakoti, and V. Reddy Kota, "Performance analysis of ANN based Multilevel-UPQC under Faulty and Overloading Conditions," *Int. J. Ambient Energy*, vol. 42, no.13, pp.1516–1528, 2019.
9. K. B. Rai, N. Kumar, and A. Singh, "Design and analysis of Hermite function-based artificial neural network controller for performance enhancement of photovoltaic-integrated grid system," *Int. J. Circuit Theor. Appl.*, vol. 51, no. 3, pp. 1440–1459, 2023. [CrossRef]
10. B. Ferdi, C. Benachaiba, S. Dib, and R. Dehini, "Adaptive PI control of dynamic voltage restorer using fuzzy logic," *J. Electr. Eng. Theor. Appl.*, vol. 1, no. 3, 2010.
11. S. B. Q. Naqvi, and B. Singh, "An enhanced filtering generalized integrator-based control for improved performance of a Grid-Tied PV system at adverse grid voltages," *IEEE Trans. Ind. Electron.*, vol. 70, no. 12, pp. 12376–12386, 2023. [CrossRef]
12. P. Kumar, S. R. Arya, and S. Kumar, "Adaptive fuzzy integrated LMS based control strategy for voltage power quality enhancement," *Electron. Energy*, vol. 9, 2024. [CrossRef]
13. P. Kumar, S. R. Arya, K. D. Mistry, and P. Ray, "Performance of DVR using diffusion norm penalized LMS fourth adaption algorithm with optimized FOPID gains," *IEEE Trans. Autom. Sci. Eng.*, pp. 1–10, 2024. [CrossRef]
14. P. Kumar, S. R. Arya, and K. D. Mistry, "TSKARNA-norm adaption based NLMS with optimized fractional order PID controller gains for voltage power quality," *Chin. J. Electr. Eng.*, vol. 9, no. 3, pp. 84–98, 2023. [CrossRef]
15. S. R. Arya, K. D. Mistry, and P. Kumar, "Least mean mixed norm square/fourth adaptive algorithm with optimized FOPID gains for voltage power quality mitigation," *IEEE J. Emerg. Sel. Top. Power Electron.*, vol. 11, no. 3, pp. 2632–2640, 2023. [CrossRef]
16. U. M. Al-Saggaf, M. Moinuddin, and A. Zerguine, "An efficient least mean squares algorithm based on q-gradient," in *Proc.48th Asilomar Conference on Signals, Systems and Computers*, 2014, pp. 891–894. [CrossRef]
17. T. Ernst, *A Comprehensive Treatment of q-Calculus*. Springer Basel, 2012.
18. K. Vanchinathan, and N. Selvaganesan, "Adaptive fractional order PID controller tuning for brushless DC motor using Artificial Bee Colony algorithm," *J. Optim.*, vol.4, no. 10, 2021. [CrossRef]
19. S. Ekinci, B. Hekimoğlu, A. Demirören, and S. Kaya, "Harris Hawks optimization approach for tuning of FOPID controller in DC-DC buck converter," International Artificial Intelligence and Data Processing Symposium (IDAP), Malatya, Turkey, vol. 2019, 2019, pp. 1–9. [CrossRef]
20. S. K. R. Priyadarshani, and J. K. Subhashini, "Satapathy, "Path Finder Algorithm Optimized Fractional Order Tilt-Integral-Derivative (Fotid) Controller for Automatic Generation Control of Multi-source Power System, "," *Microsyst. Technol.*, vol. 27, pp. 23–35, 2022.
21. M. Ali, H. Kotb, K. M. Aboras, and N. H. Abbasy, "Design of cascaded PI-fractional order PID controller for improving the frequency response of hybrid microgrid system using gorilla troops optimizer," *IEEE Access*, vol. 9, pp. 150715–150732, 2021. [CrossRef]
22. P. Trojovský, and M. Dehghani, "Pelican optimization algorithm: A novel nature-inspired algorithm for engineering applications," *Sensors (Basel)*, vol. 22, no. 3, p. 855, 2022. [CrossRef]

Prashant Kumar earned an M.Tech in power systems from SRM University in Kattankulathur, India, in 2013 after graduating with a B.Tech in electrical engineering from Hooghly Engineering and Technology College in Hooghly, India, in 2009. In 2023, the Sardar Vallabhbhai National Institute of Technology in Surat, India, awarded him a Ph.D. in electrical engineering. His areas of interest are specialized power device design, power quality, and machine learning applications.

B.E. in electrical engineering from Government Engineering College, Jabalpur, India, in 2002, M.Tech. in power electronics from Motilal Nehru National Institute of Technology, Allahabad, India, in 2004, and the Ph.D. in electrical engineering from IIT Delhi, New Delhi, India, in 2014, were conferred upon Sabha Raj Arya (Senior Member, IEEE). His areas of study are power quality and power electronics.

APPENDIX-A

Simulation parameters for DVR

Non-ideal AC line voltage (v_{sabc}) 415V, 50 Hz; Linear load = 20kVA with 0.75p.f. (lagging); ac link terminal voltage (V_t) = 339V; dc link voltage (V_{dc}) = 300V; dc bus Capacitor (C_{dc}) =4700μF; Injecting transformer 6kVA, 150/100V; Source impedance (Z_s) R = 0.060Ω, L = 5mH; Series Interfacing inductance (L_{se}) = 1.3mH; Ripple filter R_f =6Ω, C_f =10μF.

Hardware setup parameters for DVR

Non-ideal AC line voltage (v_{sabc}) 110V, 50 Hz; Linear load = 0.353 kVA with 0.66p.f. (lagging); AC bus voltage (V_t) = 90V; DC link voltage (V_{dc}) = 70V; DC bus Capacitor (C_{dc}) = 3500μF; Injecting transformer 4 kVA, 35/35V; Series interfacing inductance (L_{se}) = 0.5 mH; Ripple filter R_f = 10Ω, C_f = 120 μF; and Switching frequency = 10 kHz.